Journal of Thermal Engineering
Web page info: https://jten.yildiz.edu.tr
DOI: 10.18186/thermal.1243512

Research Article

Field-synergy and nanoparticle's diameter analysis on circular jet impingement using three oxide–water-based nanofluids

Abanti DATTA[1]*, Pabitra HALDER[1]

[1]*Indian Institute of Engineering Science and Technology, Shibpur, Howrah, West Bengal, 711103, India*

ARTICLE INFO

Article history
Received: 07 May 2021
Accepted: 12 September 2021

Keywords:
Field Synergy; Nanoparticle Diameter; Nanoparticle Concentration; Al_2O_3; TiO_2 and CuO; Circular Jet Impingement; Heat Transfer

ABSTRACT

The field synergy study is carried out using three oxide nanofluids impinging circular jet on the horizontal circular disc to analyse the synergetic interaction of cooling processes between temperature and flows fields. Theh eat transfer effect o f the nanofluid is examined by r ising the Reynolds number and the nanoparticle concentration depending on field synergy number. For jet impinged cooling process, the scale of synergy between the nanofluid flow speed and temperature is decayed with the increase of Reynolds number. Hence, it is contributed to a lower heat transfer efficiency of the nanofluid. Whe reas, the scale of synergy between the nanofluid flow speed and temperature can be enhanced by rising the particle concentration. Thus, the heat transfer efficiency of the nanofluid is incr eased. Analysis showed that Al_2O_3 nanofluid has the maximum relative field synergy among selected three oxide nanofluids. It is evident that the nanoparticle concentration, nanoparticle material and Reynolds number have significant effect on the heat transfer augmentation. In addition, the study is explored by varying jet-disk spacing. Moreover, the investigation has shown that the reducing heat transfer effect for the materials is Al_2O_3, CuO and TiO_2 subsequently. It is revealed that the heat enhancement is higher for smaller nanoparticle's diameter (i.e., 20 nm) than bigger nanoparticle's diameter (i.e., 80 nm) of the same material.

Cite this article as: Datta A, Halder P. Field-synergy and nanoparticle's diameter analysis on circular jet impingement using three oxide–water-based nanofluids. J Ther Eng 2023;9(1):179–190.

INTRODUCTION

Jet impingement cooling is very efficient in the case of the elimination of the maximum heat and the conservation of the minimum temperature. In addition, the jet flow determines its individual flow direction, so additional channelling is not needed to cool. Furthermore, the cooling of jet impingement has the ability to minimize maximum heat flows when the speed of the jet is under high pressure of stagnation. Impinging jet applications can be used in

***Corresponding author.**
*E-mail address: abanti.datta@gmail.com

This paper was recommended for publication in revised form by Regional Editor Patrice Estellé

Published by Yıldız Technical University Press, İstanbul, Turkey

many industries, including gas turbine cooling, paper and textile drying, cooling rocket launcher, electrical cooling systems, steel or glass, and many others.

Recent researchers have drawn attention to the dispersion of nanoparticles into specific fluid to be used in impinging jets. Roy et al. [1] conducted numerical analysis on Al2O3-water nanofluid to investigate hydrodynamic and thermal fields in the laminar region. They described that heat transmission improved by 200 percent with nanofluid dispersed by 10 percent at Re=1200. The forced convective flow of nanofluids using Al_2O_3-water is numerically analysed by Palm et al. [2]. They recorded an increase of 25 percent in the average heat transfer coefficient of 4 percent volume fraction of nanoparticle. Roy et al. [3] has analyzed numerically the radial laminar flow of nanofluids for electronic cooling applications in a simplified axisymmetric configuration. Yang and Lai [4] have numerically investigated with temperature independent properties of water-alumina nanofluid. Whereas Yang and Lai [5] investigated with temperature dependent properties of same nanofluid. Both of them carried out their simulations on confined jet impingement. They have concluded that Nusselt number is increased as the Reynolds number increases. Even volume concentration of nanofluid has a significant effect no Nu No. Feng and Kleistreur [6] have numerically studied on two parallel disks. Since they have used water-alumina as a nanofluid, the results showed same trend as [4] and [5]. Feng and Kleistreur [6] further studied different case by varying nanoparticles concentration, spacing between disks. As the spacing between disks is increased the Nu no decreased and for larger nanoparticles Nu no is diminished. Gherasim et al. [7] studied the restrictions of confined radial flow of impinging jet. The jet consists of water=alumina nanofluid and flow is laminar regime. Vaziei and Abouali [8] also have numerically studied on confined circular jet. They have investigated on both laminar and turbulent flow of jet impingement. It was concluded that laminar jet had greater effect than turbulent one in heat transfer enhancement. Roy et al. [9] numerically studied on laminar steady flow regime with impinging jet. Also, Palm et al. [2] studied on laminar flow however with two parallel disks. They kept the constant properties of nanofluid (water-alumina). Some experimental results are discussed here where water-alumina is used as nanofluid. Sagot [10] is carried out experimental study to investigate heat transfer capabilities by varying disk to jet spacing. He studied different case by altering Reynolds No. (i.e., 15000 and 30000). He reported that wider jet-disk spacing reduces the heat transfer capacities. Nguyen et al. [11] has experimented between confined jet and circular heated horizontal surface. They have studied on both laminar and turbulent flows of water-alumina nanofluid. The previous literatures concluded that water-alumina nanofluid (4% of volumetric concentration) improved the heat transfer enhancement nearly by 25 percent than water (used as coolant). Eiamsaard and Kiatkittipong [12] experiment is showed that the thermal efficiency is higher TiO_2 -water nanofluid compare to the use of pure water. Ahmed and Eslamian [13] studied on CuO-water nanofluids. They have found that at lower Reynolds number convection heat transfer coefficient is increased and vice versa. Goudarzi et al. [14] conducted a study on solar collector using both distilled water and CuO-water nanofluid. The results demonstrate that thermal efficiency is increased drastically for CuO-water nanofluids.

Based on the insights garnered from the available literature, it appears to be a significant requirement for the equations that explain and determine heat transfer coefficients for jet impingement, and hence electrical cooling systems. Heat transfer coefficients are affected by the Prandtl number and the Reynolds number, as well as the physical features of nanoparticles and base fluids. This article focused on the effect of heat transfer improvement by altering jet-disk spacing, Reynold number and volumetric concentration. Numerical simulation is carried out in axisymmetric configuration between horizontal heated round disk and vertical confined jet impingement. Metal or metal oxide nanoparticles are commonly used in nanofluids and Al_2O_3, TiO_2 and CuO are the most frequently used nanoparticles. So, authors have decided to take these three nanoparticles. As per authors' knowledge, numerical results are scarcely reported on impact of nanoparticle's diameter and material on circular jet impingement in in a turbulent regime with addition of scale of field synergy. The thermo-physical properties of three nanofluid is programmed using User-Defined Functions (UDF) of ANSYS Fluent. Authors have studied 3 cases with nanoparticles material of aluminium oxide, titanium dioxide and copper oxide and particle diameter size range of 20, 40 and 80 nm. Reynolds No. 10000, 20000, 40000 and particle concentration of 1%, 2% and 4% are considered for to evaluate thermal and fluid dynamic behaviour, adopting a single-phase approach. And simulations are done at two jet-disk spacing (H/D) as 1 and 5.

MATHEMATICAL MODELLING

Problem Description

Figure 1 is showed the axisymmetric flow domain and mesh, is analysed numerically to measure heat transfer efficiency same as Sagot et al. [10]. The nanofluid jet is impinged on the circular disc of radius R. The jet diameter is D and the distance between jet and disc is H. The jet is impacted with a flow speed at U and temperature, T_j is 298K. The top surface of the region would be expected to be an adiabatic wall, while bottom surface is kept as isothermal wall with temperature, T_w, 348 K. The left-hand side of boundary is assumed to be symmetrical boundary and the right-hand side of boundary is pressure outlet.

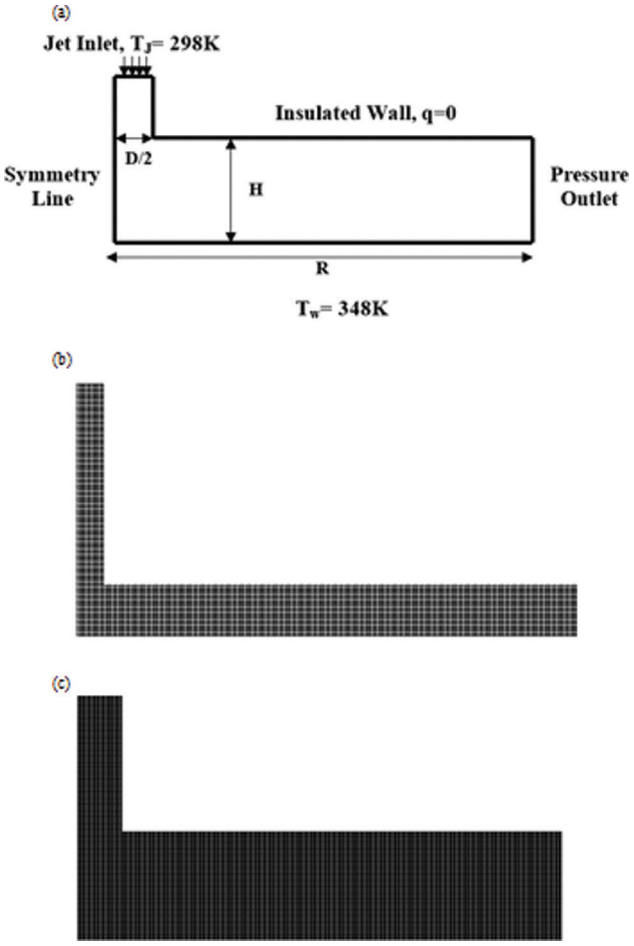

Figure 1. Diagram of schematic diagram of impinging jet with boundary conditions (a), Mesh diagram for H/D = 1 (b), Mesh diagram for H/D = 5 (c).

Governing Equations and Turbulence Modelling Equations

A single-phase technique was used in the present study to model the water-Al_2O_3 nanofluid. A hydrodynamic and thermal equilibrium was postulated between the base fluid and solid particles, with no-slip velocity between the fluid phase and solid phase. As a result of this assumption, the mixture of water and nanoparticles was handled as a homogenous phase when the volumetric fraction of the nanoparticles was relatively small. The jet was considered to be steady, turbulent, two-dimensional, and no buoyancy forces. Aside from that, the impacts of heat transmission via viscous dissipation and radiation were ignored.

To carry out the present simulation, it is assumed that the mixture is single-phase fluid with improved the properties because of the accumulation of nanoparticles with different volume fraction. The governing equations are stated as:

$$\frac{\partial U_i}{\partial x_i} = 0 \tag{1}$$

$$\rho U_i \frac{\partial U_j}{\partial x_i} = -\frac{\partial P}{\partial x_j} + \frac{\partial}{\partial x_i}\left[\mu\left(\frac{\partial U_i}{\partial x_j} + \frac{\partial U_j}{\partial x_i}\right) - \rho\overline{u_i' u_j'}\right] \tag{2}$$

$$\rho C_p U_i \frac{\partial T}{\partial x_i} = \frac{\partial}{\partial x_i} k\frac{\partial T}{\partial x_i} - \rho\overline{u_i' T'} \tag{3}$$

$$-\rho\overline{u_i' u_j'} = \mu_t\left(\frac{\partial U_i}{\partial x_j} + \frac{\partial U_j}{\partial x_i}\right) - \frac{2}{3}\delta_{ij}\rho\lambda \tag{4}$$

In this equation U_i is the velocity component in the direction x_i while P and T are the pressure and temperature component respectively. And ρ, C_P and K are the density, the heat capacity and the thermal conductivity respectively. According to the momentum equation (2), the turbulent Reynolds stresses $\rho\overline{u_i' u_j'} = \mu_t$ are equal to the turbulent heat transfer flux and the turbulent heat transfer flux is equal to $\rho\overline{u_i' T'}$ in the energy equation (3) using an opposite turbulence model. μ_t is denoted as the turbulent viscosity and δ_{ij} is denoted as the Kronecker symbol. λ is the turbulent kinetic energy. According to Reference [15], the turbulent Reynolds stresses and turbulent heat transfer were calculated using the eddy viscosity models.

In order to determine the turbulence behaviour of turbulent flows, k-w SST turbulence model is used. This turbulence model is suggested by Menter [16]. The two equations are the Turbulence Kinetic Energy and the Specific Dissipation Rate respectively:

$$\frac{\partial k}{\partial t} + U_j\frac{\partial k}{\partial x_j} = P_k - \beta * k\omega + \frac{\partial}{\partial x_j}\left[(n + \sigma_k n_T)\frac{\partial k}{\partial x_j}\right] \tag{5}$$

$$\frac{\partial \omega}{\partial t} + U_i\frac{\partial \omega}{\partial x_j} = \alpha S^2 - \beta\omega^2 + \frac{\partial}{\partial x_j}\left[(n + \sigma_\omega n_T)\frac{\partial \omega}{\partial x_j}\right] + 2(1 - F_1)\sigma_{\omega 2}\frac{1}{\omega}\frac{\partial k}{\partial x_j}\frac{\partial \omega}{\partial x_j} \tag{6}$$

A coarse mesh can produce good results as long as the boundary region is well resolved. Because of the turbulent flow, the heat transmission on the target plate is affected. The numerical results vary depending on which Turbulence Model is chosen. In spite of this, the k-ω SST turbulence model provides a suitable quantitative distribution of the results as the optimum balance between computing cost and accuracy.

Thermo-Physical Properties of Nanofluids

The nanofluid density and nanofluid specific heat [17] equations are (7) and (8) respectively. Equation (9) and Equation (10) are gotten from regression analysis of experimental results [18]. The nanoparticles of Al_2O_3, TiO_2 and CuO with diameter range of 20 to 80 nm are considered. The base fluids are water. The suffices bf and nf is to indicate base fluid and nanofluids respectively. $T_{bf\text{-}f}$ is denoted as freezing point of water, 273.15 K. The physical properties of all nanoparticles are given in Table 1.

$$\rho_{nf} = (1-\varphi)\rho_{bf} + \varphi\rho_p \tag{7}$$

$$\rho_{nf}Cp_{nf} = (1-\varphi)\,\rho_{bf}Cp_{bf} + \varphi\rho_p Cp_p \tag{8}$$

$$K_{nf} = K_{bf}1 + 4.4Re^{0.4}Pr^{0.66}\left(\frac{T_{nf}}{T_{bf-f}}\right)^{10}\left(\frac{k_p}{k_{bf}}\right)^{0.03}\varphi^{0.66} \tag{9}$$

$$\mu_{nf} = \frac{\mu_{bf}}{1-34.87\left(\frac{d_p}{d_{bf}}\right)^{-0.3}\varphi^{1.03}} \tag{10}$$

Assumptions

Steady-state, turbulent, incompressible and constant properties flow conditions are assumed in the present analysis. Adopting single phase model for the nanofluid and considering thermal equilibrium after evaluating the thermos-physical properties of the nanofluid using mentioned equation and some assumptions are taken as follows:

- Flow is Newtonian, incompressible and turbulent.
- Nanofluid comprising of two phases is homogeneous.
- Viscous dissipation is negligible.
- Shape and size of nanoparticles are uniform and spherical.

Concept of Field Synergy

Researchers have attempted to describe mechanisms to improve nanofluid heat transfer. A new concept for understanding the mechanism of heat exchange using nanofluid is the field synergy concept developed by Guo et al. [22]. They incorporated the energy equation of the boundary layer into the thermo boundary layer thickness and found that the temperature gradient on the outside boundary is zero and the internal convection term is calculated from internal speed and temperature gradient.

The smaller angle between the speed and the temperature gradient is produced the higher the heat transfer rate for a constant flow field and temperature difference. The concept is referred to as the field synergy theory.

The theory of field synergy is also aided by Bergles [23]. The energy equation:

$$\rho C_p\left(u\frac{\partial T}{\partial x} + v\frac{\partial T}{\partial y}\right) = \frac{\partial}{\partial y}\left(k\frac{\partial T}{\partial y}\right) \tag{11}$$

The energy equation with boundary layer thickness:

$$\int_0^{\delta_t}\rho C_p\left(u\frac{\partial T}{\partial x} + v\frac{\partial T}{\partial y}\right)dy = -k\frac{\partial T}{\partial y}\bigg|_w = q_w \tag{12}$$

where δ_t is denoted as thermo boundary layer thickness.

The energy equation in vector form:

$$\int_0^{\delta_t}\rho C_p(u\nabla T)dy = -k\frac{\partial T}{\partial y}\bigg|_w = q_w \tag{13}$$

where,

$$\bar{U} = \frac{u}{u_\infty} \tag{14}$$

$$\nabla\bar{T} = \frac{\nabla T}{(T_\infty - T_w)/\delta_t} \tag{15}$$

Equation (13) can be rewritten as per [23, 25]:

$$Nu = RePr\int_0^1(\bar{U}.\nabla\bar{T})d\bar{y} \tag{16}$$

It is found from equation (16) that Nu can be calculated from Re, Pr and the integral term. Tao et al. [25] have reported that under perfect synergistic conditions, the term RePr is equal to Nusselt number (i.e., the isotherms are perpendicular to the vectors). Nevertheless, Re and Pr are

Table 1. Thermo-physical properties of nanoparticles and water at 300K

Material	ρ(kg/m3)	Cp (J/kg K)	μ (Pa s)	K (W/m K)	Reference
Water	998.2	4182	998 ×10−6	0.597	Datta & Halder [19]
Al_2O_3	3880.0	773	-	36.0	Datta & Halder [20]
CuO	6320	532	-	18	Sahoo & Sarkar [21]
TiO_2	4157	692	-	8.4	Sahoo & Sarkar [21]

often controlled by operating conditions such as the provided flow rate, H/D ratio, pumping capacity and working fluid. The effective method of improving heat transfer is to increase the integral form, i.e. synergy number (Fc). For most convective heat transmission matters, Fc =1 under maximum synergy conditions and is much smaller than 1, suggesting a wide room for heat transmission.

The dimensionless expression (Guo et al. [22, 24]) from equation (16) is:

$$F_c = \frac{Nu}{RePr} = \int_0^1 (\bar{U}.\nabla\bar{T})d\bar{y} \tag{17}$$

Here F_C is dimensionless field synergy number. This number is denoted as scale of field synergy for entire flow field and this number can be defined as scale of field synergy among the flow field and temperature gradient. Depending on the heat transfer surface form, the value may be differed from 0 to 1. This is the full interpretation of "field synergy" terms. Comprehensive work has been carried out to develop technology for the improvement of the heat transfer. The analysis for field synergy number is emphasized to dictate the intersection of speed and temperature gradient vectors and find local convection rate for a Reynolds number and jet to disc distances with constant heat flux.

BOUNDARY CONDITIONS, GRID SENSITIVITY AND MODEL VALIDATION

The jet is impinged on the disc with a speed, U and temperature, T_J = 298 K. The boundary condition is applied on the left side of the domain is symmetry boundary and on the right side of the domain is pressure outlet. The temperature, TW= 348 K is kept at the disc. The boundary conditions were used to solve the continuity, momentum and energy equations (1) to (4). The inlet jet exit had uniform velocity and temperature profiles; the exit sections had pressure outlets; the upper wall had an adiabatic wall and no-slip velocity; and the impinged wall had constant temperature. Turbulence intensity and length scale at the inlet jet were set to 2%.

At the jet inlet boundary, a uniform axial velocity and temperature profile is considered,

$$U = U_J : T = T_J \tag{18}$$

At left hand side boundary,

$$U = 0 : \partial U_r/\partial r = \partial T/\partial r = 0 \tag{19}$$

On the upper disk, the no-slip conditions as well as a uniform heat flux,

$$U = 0 : \ddot{q} = 0 \tag{20}$$

At impinged surface, the usual no-slip conditions insulated wall are specified,

$$U = 0 : T = T_w \tag{21}$$

At right hand side boundary,

$$P = P_{amb} \tag{22}$$

The finite method of volume is used to resolve the boundary conditions with integrated differential nonlinear equations. For numerical calculations the pressure dependent solver (ANSYS Fluent) is used. The nanofluid thermo-physical properties are coded using User- Defined Functions (UDF) of ANSYS Fluent. The energy and momentum equations are calculated by the interpolation of the second order upwind method. The solution is expected to converge, when the normalized residual decreases less than 10^{-9} for the energy terms and less than 10^{-6} for all other variables.

For k- ω SST model with the non-uniform grid, the grid sensitivity of y+=1 on viscous sublayer is presented. At Reynolds Number 30,000 and H/D=5 grid-independent analysis is carried out on four different grid distributions (240×70, 260×80, 280×90 and 300×100 – grid nodes). Since the distribution of Nusselt numbers for grid 300x100 doesn't drastically change, the simulations are carried out on grid 300x100 as shown in Figure 2.

A structured code explanation and performance evaluation of the k–ω SST models are carried out before performing on actual simulations. The simulation is conducted at uniform jet velocity equivalent to Reynolds number, 10000 and H / D =2. The comparison of the Nusselt number profile and experimental Nusselt number profile of Sagot et al. [10] was illustrated in Figure 3. The experimental configuration

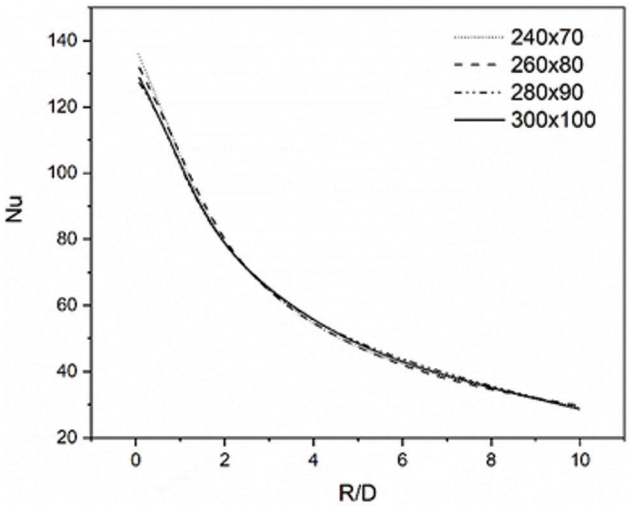

Figure 2. Grid sensitivity.

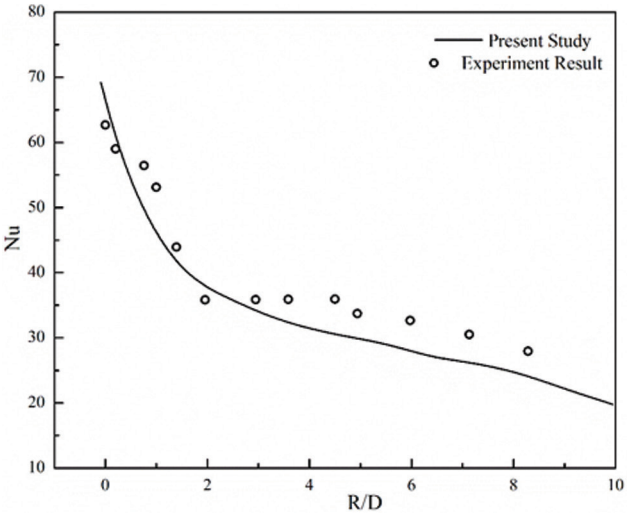

Figure 3. Validation result with Sagot [10] experimental result.

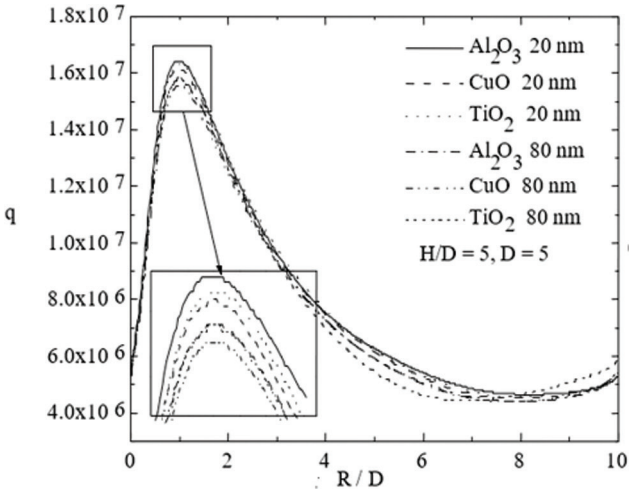

Figure 4. Effect of nanoparticle material and size at φ = 2% and Re=40000.

[11] is made up of 2.4 mm jet diameter and 24 mm disc radius. At the R / D, the value of the local Nusselt number is low at the impinged disc and then decreases with the R / D increasing. The present result for the Nusselt distribution profile is strongly endorsed with experimental result.

RESULTS AND ANALYSIS

The analysis carried out by varying nanoparticles material of Al_2O_3, CuO and TiO_2 and varying particle size of 20, 40 and 80 nm. For further investigation, Reynolds number (Re) and the H/D ratio are also varied. In order to obtain results concerning the change in fluid properties, the nanoparticle concentration has been varied as 1%, 2% and 4%. Doing this has led to obtaining results for changing geometry and nanofluid properties, as well as changing flow rates. The study also focused on synergy effect of the temperature and the velocity field to enhanced heat transfer across nanofluids.

Effect of Nanoparticle Material and Nanoparticle's Diameter

Figure 4 is showed the effects of nanoparticle material and nanoparticle size. One can see that CuO has the lowest heat transfer rate whereas Al_2O_3 has the highest heat transfer rate. The heat enhancement is more for the smaller nanoparticle's diameter i.e., 20 nm as compare to the bigger nanoparticle's diameter i.e., 80 nm of a specific material. At φ = 2% due to change of particle size from 20 nm to 80 nm heat transfer rate is decreased of 3.88 percent at the peak point. Whereas, heat transfer rate is decreased by 4.12 percent for CuO nanoparticles and for TiO_2 nanoparticles it is 3.5 percent.

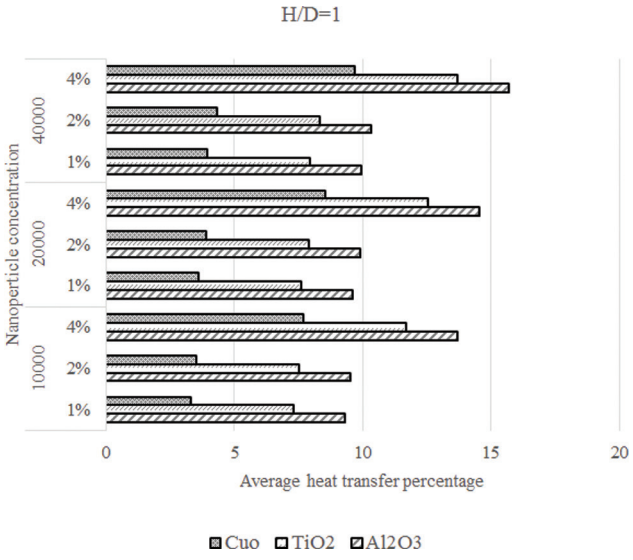

Figure 5. Percentage change of average heat transfer coefficient or H/D = 1.

Effect on Average Heat Transfer Coefficient

Figure 5 and 6 are illustrated percentage change in average heat transfer coefficient for different Reynolds number and volume concentration at fixed value of H/D = 1 & H/D = 5 respectively. It is noted that the heat transfer coefficient is chosen over non-dimensional Nusselt umber to compare thermal transfer effectiveness. It's because the Nusselt number understates the increased thermal conductivity of nanofluids in comparison. A significant augmentation in the heat transfer rate has been observed with

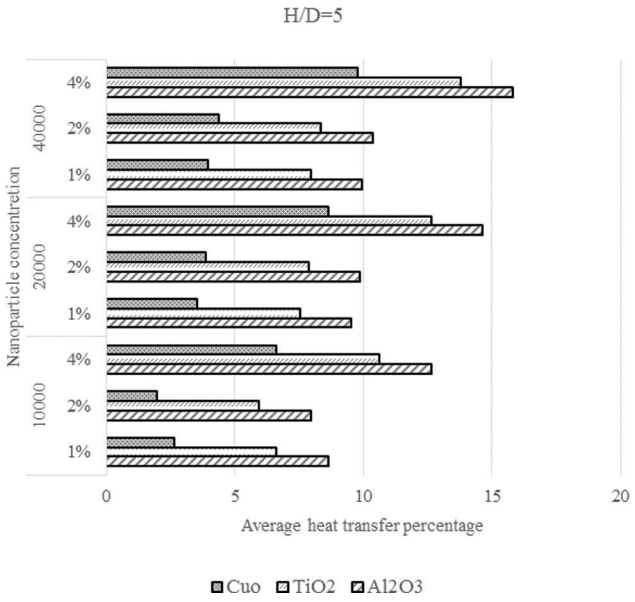

Figure 6. Percentage change of average heat transfer coefficient for H/D = 5.

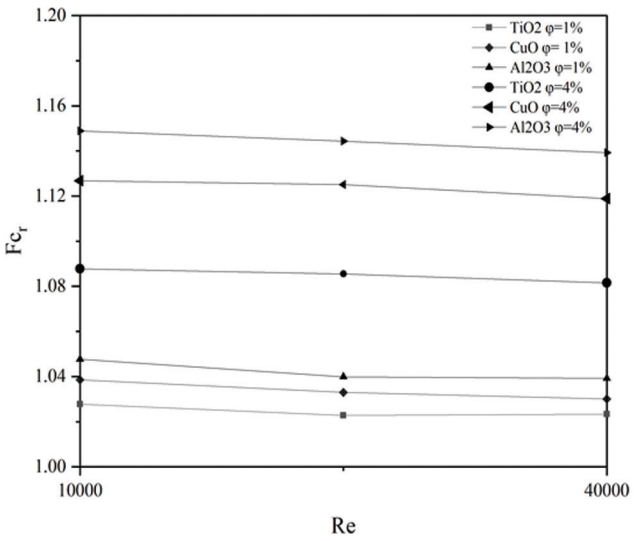

Figure 7. Relative field synergy number along with Reynolds number for TiO_2, CuO and Al_2O_3 nanofluids.

dispersion of nanoparticles in working fluid. It can be also noted that the coefficient of heat transfer is increased when Reynolds number rise. Figure 5 is showed that best thermal transfer efficiency of the Al_2O -water nanofluid compared to the other selected nanofluids. Whereas thermal transfer efficiency is least for CuO-water nanofluid. This can be explained by the Prandtl number. If the viscosity is considered to be the same for all three nanofluids, the thermal conductivity is highest for Al_2O_3 -water nanofluid. Moreover, for all Reynolds number considered in this analysis this pattern is identical.

Field Synergy Analysis

For jet impingement simulation, the equation (12) is used to calculate heat enhancement and flow characteristics. It is noted that dimensionless integration is required to increase to increase heat enhancement. The results of the simulation show that in the analysis the convective heat transfer is acquired nearly synergized across the entire domain. And Nusselt number is reached at its peak and the Reynolds number is increased in the same way. Whereas, the equation (13) is interpreted the convective energy transfer. So, the total convective heat transfer can be predicted by field synergy number.

The relative field synergy number is a ratio of field synergy number of nanofluid to field synergy number of water (Minea and Manca [26]):

$$F_{C_r} = \frac{F_{C_{nf}}}{F_{C_{bf}}} \tag{23}$$

The relative heat transfer coefficient is a ratio of heat transfer coefficient for the nanofluids to heat transfer coefficient for the base fluid: (Minea and Manca [26]):

$$h_r = \frac{h_{nf}}{h_{bf}} \tag{24}$$

Figure 7 is showed the relative field synergy number along with Reynolds number for 20nm diameter. All three different nanofluids with different volume concentration is plotted. It is noted that the field synergy number is improved with addition of nanoparticles volume concentration to water, in that way the degree of synergy is increased between the flow fields and temperature. Due to dispersion of nanoparticles in water, the synergy is increased. The lowest synergy is observed for TiO2-water nanofluid while the highest synergy is observed for Al_2O_3 -water nanofluid among three considered nanofluids. overall heat augmentation proposed that the synergy number is increased by 16 percent while heat transfer effect is enhanced by 3.6 percent for 4% concentration of Al_2O_3 -water nanofluid. The field synergy analysis is state that field synergy marginally is declined with the increased of Reynolds number for all selected nanofluids. In the case of high Reynolds, the field synergy number decreases marginally due to the fact that the rise in velocity cannot fully offset the rise in the heat transfer coefficient. Thus, field synergy number is reversed proportionate to the velocity of the fluid and directly proportionate to heat transfer coefficient.

Since Al_2O_3 nanofluid has highest heat transfer rate and maximum relative field synergy compare to other two

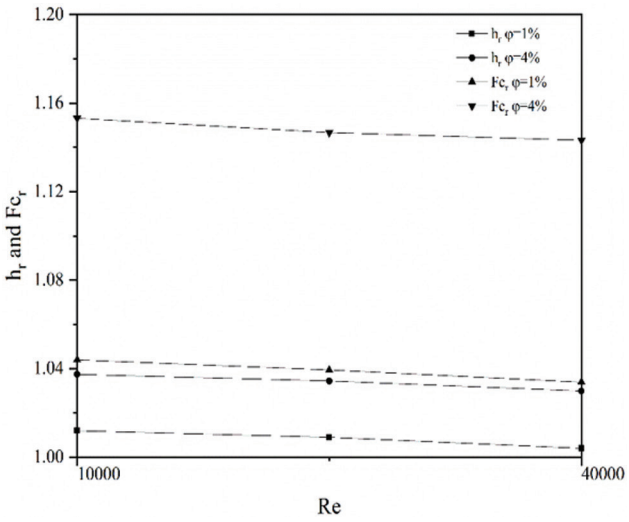

Figure 8. Relative field synergy and relative heat transfer coefficient along with Reynolds number for Al_2O_3 nanofluid.

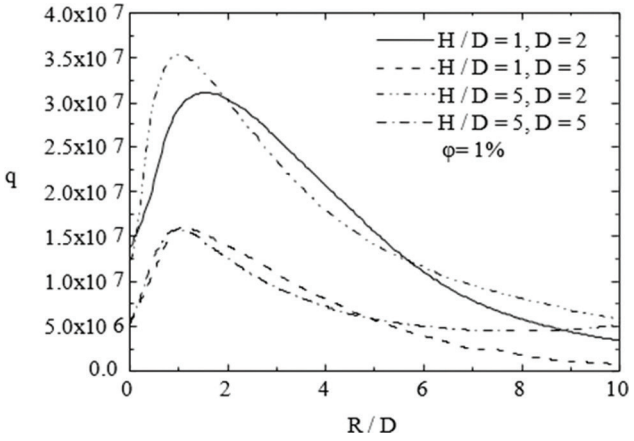

Figure 9. Heat flux, q [W/m^2] at Re=40000 and 20nm diameter for Al_2O_3 nanofluid.

nanofluids, the other parameters to enhance the heat transfer is discussed on Al_2O_3-water nanofluid.

Figure 8 is showed he comparison the relative field synergy and the relative heat transfer coefficient along with Reynolds number for Al_2O_3 nanofluid. From the Figure 8, it can be determined that the relative field synergy for the same nanofluid concentration is greater than the relative heat transfer and it is degrade with an increase of Reynolds number. It is also determined that with rise of nanofluid concentration, the differences are greater. The increase in heat conductivity and the surge in the nanofluid Viscosity compared to water can be explained by this phenomenon. So, it can be concluded that relative synergy is consistent with the observed trend towards the increase in the heat transfer coefficient and hence the concept of field synergy assists as an important technique in the design of convective heat transfer equipment.

Effect of Changing Nozzle Diameter

Figure 9 is illustrated the effects of variation of the jet diameter, D and distance between jet nozzle to impinged disc, H/D ratio for Al_2O_3 nanofluid. At fixed H/D ratio if D is enlarged, H is increased too. Due to increase of jet diameter for the same H/D ratio the heat transfer rate is decreased. And the heat transfer rate is increased while jet diameter is reduced at fixed H/D ratio. For H/D= 1, the peak value of the heat transfer is decreased by 95 percent when jet diameter is enlarged from 2 mm to 5 mm. At H/D = 5, for the same rise of jet diameter the change is 124 percent. Whereas, changing H/D ratio for same jet diameter is caused the peak value of heat transfer rate to shift towards the center of the disc on the left-hand side.

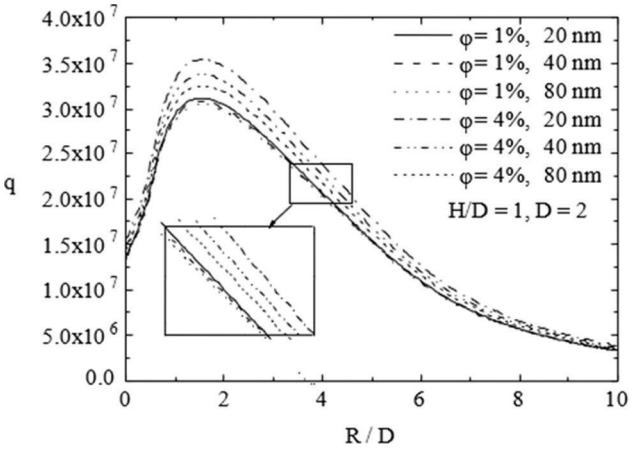

Figure 10. Effect of nanoparticle's diameter at Re=40000 for Al_2O_3 nanofluid.

Effect of Nanoparticle's Diameter

Figure 10 is demonstrated that how nanofluid's dispersion fraction and nanoparticle's diameter is interrelated for Al_2O_3 nanofluid. The increasing size of nanoparticle has seen to have a reverse impact on heat propagation. For higher concentrations, this shift is prevalent. When concentration is increased from 1% to 4%, the peak point of heat enhancement profile is changed 7 percent, 10 percent and 14 percent for 80 nm, 40 nm and 20 nm respectively. The decrease of the size of the nanoparticles from 80 nm to 20 nm for 1 percent reduces heat transfer at peak point of 2 percent, while this decrease is 9 percent for 4 percent concentrations. It can be inferred that the particle diameter has a significant impact in the nanofluid jet impingement.

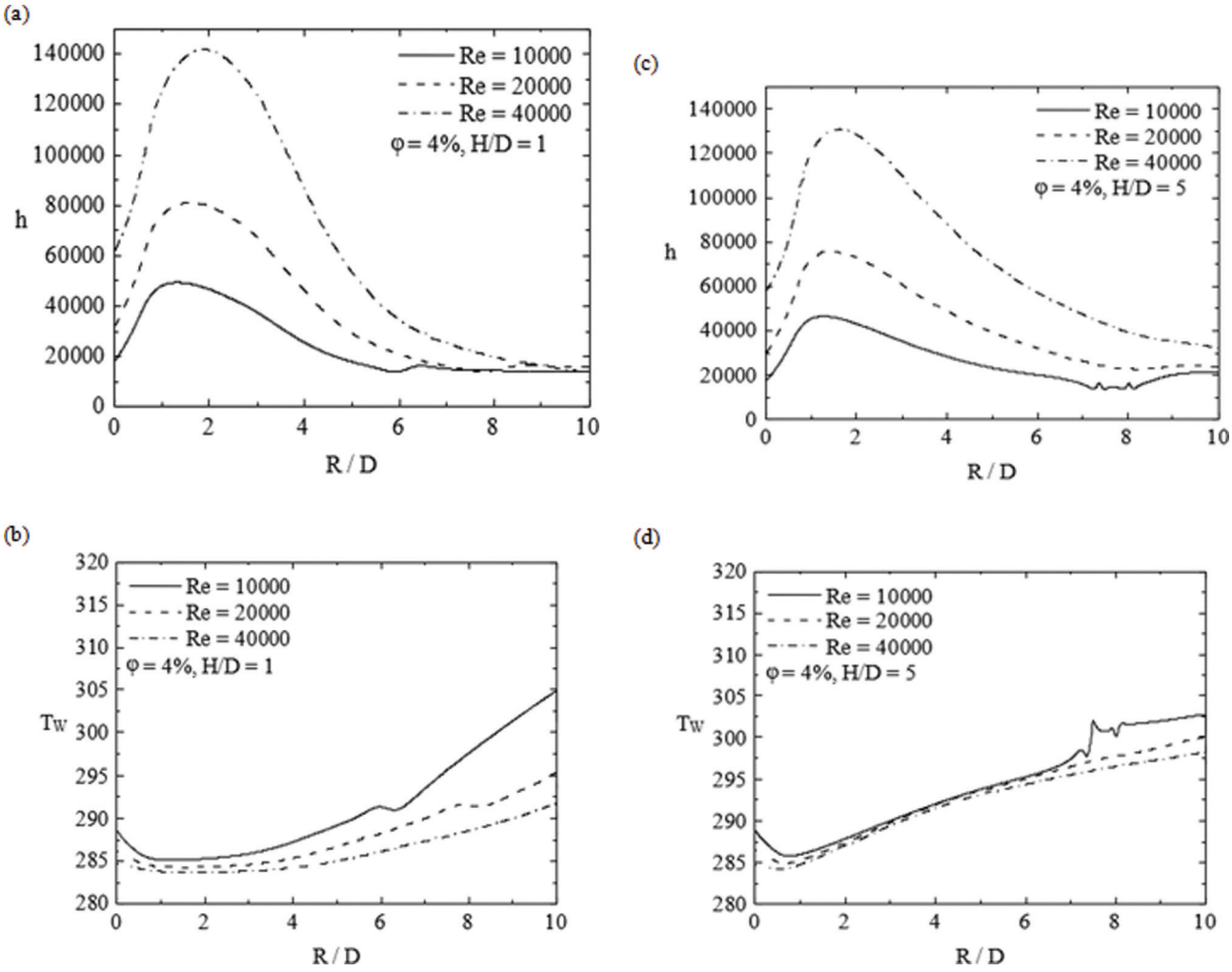

Figure 11. Effect of φ= 4%with H/D= 1 and H/D = 5 for Al_2O_3 nanofluid (Heat transfer coefficient, h [W/m²K] (a), Plate temperature, T_W [K] (b), Heat transfer coefficient, h [W/m²K] (c), Plate temperature, T_W [K] (d)).

Effect of Changing Nanoparticles Concentration

Figure 11 (a and c) shows the effect of increasing nanoparticles concentration with same nanofluid properties and geometry for Al_2O_3 nanofluid. It is seen that increasing nanoparticles concentration causes heat transfer coefficient increased. Also, the peak of each profile is seen to shift away from the plate center with increasing nanoparticles concentration. Figure 11 (b and d) shows the plate temperature with increasing nanoparticles concentration for Al_2O_3 nanofluid.

The figures of the temperature fields and streamlines contours are presented in Appendix A1(a and b) and A3 (a and b) & A2(a and b) and A4(a and b) respectively, for φ=4% the representative cases with H/D = 1 and 5, at Re = 10000 and 40000. Hereafter, the overall results for different Reynolds number are concluded. Figure A1 and A3 & A2 and A4 show the variations temperature and streamlines field at different h/W ratios and Reynolds numbers in the flow field of Al_2O_3 -water nanofluids along the bottom surface.

CONCLUSIONS

The effect of nanoparticles materials in heat transfer enhancement is in the decreasing order of Al_2O_3, CuO and TiO_2. Field synergy analysis is well represented the heat enhancement properties and the fluid flow structure of the nanofluids and which results in an improved heat transfer mechanism. It is observed that the field synergism number is surged under turbulent flow conditions as the concentration in nanofluid is increased. However, the field synergism number is decreased as the Reynold number increased. The increase in heat transfer can be ascribed in accordance with the field synergy analysis to the improving synergy between

the velocity structure and temperature field. The field synergy analysis therefore provides a basis for understanding of the heat augmentation phenomena using nanofluids. The highest synergy is attributed for Al_2O_3-water nanofluid among three considered nanofluids. Therefore, the other parameters to enhance the heat transfer is discussed on Al_2O_3-water nanofluid only.

It is observed that for same H/D ratio and increasing nozzle diameter, the heat transfer rate is changed significantly as it is subject to jet velocity and turbulent intensity. It is also noted that the peak point of the heat transfer is shifted towards the plate center. Whereas, for same nozzle diameter and increasing H/D ratio the temperature is raised at near the impingement surface and decreased at edge of plate. Due to increment of nanoparticle dispersion, the fluid bulk temperature is increased which is elevated heat propagation of the mixture. Again, for same dispersion and increasing nanoparticle size the heat transfer rate is decreased; this is more influential for higher dispersion of nanoparticles. In addition, the increase of Reynold number as well as accumulation of nanoparticle dispersion has been shown to enhance the heat transfer compared to the pure water.

NOMENCLATURE

D	diameter of jet
H	distance between slot and heated plate
R	radius of the round plate
U	inlet velocity of jet
T_J	inlet temperature of jet
T_w	temperature of heated plate
C_p	specific heat
Re	Reynolds number
Nu	Nusselt number
k	turbulent kinetic energy
H	enthalpy
U_i	velocity component in the direction x_i
Pr	Prandtl number
P	pressure
T	temperature
K	thermal conductivity
F_C	dimensionless field synergy number
P_{amb}	ambient pressure
h	heat transfer coefficient
q	Heat flux

Greek letters

ρ	density
φ	volume concentration of nanoparticles
δ_{ij}	Kronecker symbol
μt	turbulent viscosity
ω	specific dissipation rate of k
λ	turbulent kinetic energy
δ_t	thermo boundary layer thickness.

Subscripts

nf	nanofluid
bf-f	freezing point of water
bf	base fluid
p	nanoparticles

AUTHORSHIP CONTRIBUTIONS

Authors equally contributed to this work.

DATA AVAILABILITY STATEMENT

The authors confirm that the data that supports the findings of this study are available within the article. Raw data that support the finding of this study are available from the corresponding author, upon reasonable request.

CONFLICT OF INTEREST

The author declared no potential conflicts of interest with respect to the research, authorship, and/or publication of this article.

ETHICS

There are no ethical issues with the publication of this manuscript.

REFERENCES

[1] Roy G, Nguyen CT, Lajoie PR. Numerical investigation of laminar flow and heat transfer in a radial flow cooling system with the use of nanofluids. Superlattices Microstruct 2004;35:497–511. [CrossRef]

[2] Palm SJ, Roy G, Nguyen CT. Heat transfer enhancement with the use of nanofluids in radial flow cooling systems considering temperature-dependent properties. Appl Therm Eng 2006;26:2209–2218. [CrossRef]

[3] Roy G, Nguyen CT, Comeau M. Numerical investigation of electronic component cooling enhancement using nanofluids in a radial flow cooling system. J Enhanc Heat Transf 2006;13:101–115. [CrossRef]

[4] Yang YT, Lai FH. Numerical study of heat transfer enhancement with the use of nanofluids in radial flow cooling system. Int J Heat Mass Transf 2010;53:5895–5904. [CrossRef]

[5] Yang YT, Lai FH: Numerical investigation of cooling performance with the use of Al2O3/water nanofluids in a radial flow system. Int J Thermal Sci 2011;50:61–72. [CrossRef]

[6] Feng Y, Kleinstreuer C. Nanofluid convective heat transfer in a parallel disk system. Int J Heat Mass Transf 2010;53:4619–4628. [CrossRef]

[7] Gherasim I, Roy G, Nguyen CT, Vo-Ngoc D. Heat transfer enhancement and pumping power in confined radial flows using nanoparticle suspensions (nanofluids). Int J Therm Sci 2011;50:369–377. [CrossRef]

[8] Vaziei P, Abouali O. Numerical study of fluid flow and heat transfer for Al2O3-water nanofluid impinging jet. In: editor. Proceedings of the 7th International Conference on Nanochannels, Microchannels and Minichannels; 2009 Jun 22-24; Pohang: American Society of Mechanical Engineers; 2009. pp. 977–984. [CrossRef]

[9] Roy G, Palm SJ, Nguyen CT. Heat transfer and fluid flow of nanofluids in laminar radial flow cooling sys-tems. J Therm Sci 2005;14:362–367. [CrossRef]

[10] Sagot B, Antonini G, Christgen A, Buron F. Jet impingement heat transfer on a flat plate at a constant wall temperature. Int J Therm Sci 2008;47:1610–1619. [CrossRef]

[11] Nguyen CT, Galanis N, Polidori G, Fohanno S, Popa CV, Le Bechec A. An experimental study of a confined and submerged impinging jet heat transfer using Al2O3-water nanofluid. Int J Therm Sci 2009;48:401–411. [CrossRef]

[12] Eiamsa-ard S, Kiatkittipong K. Heat transfer enhancement by multiple twisted tape inserts and TiO2/water nanofluid. Appl Therm Eng 2014;70:896–924. [CrossRef]

[13] Ahmed M, Eslamian M. Laminar forced convection of a nanofluid in a microchannel: Effect of flow inertia and external forces on heat transfer and fluid flow characteristics. Appl Therm Eng 2015;78:326–338. [CrossRef]

[14] Goudarzi K, Shojaeizadeh E, Nejati F. An experimental investigation on the simultaneous effect of CuO–H2O nanofluid and receiver helical pipe on the thermal efficiency of a cylindrical solar collector. Appl Therm Eng 2014;73:1236–1243. [CrossRef]

[15] ANSYS Fluent 12.0 user's guide, Ansys Inc. 2009;15317:1–2498.

[16] Menter FR. Two-equation eddy-viscosity turbulence models for engineering applications. AIAA J 1994;32:1598–1605. [CrossRef]

[17] Buongiorno J. Convective transport in nanofluids. J Heat Transf 2006;128:240–250. [CrossRef]

[18] Corcione M. Empirical correlating equations for predicting the effective thermal conductivity and dynamic viscosity of nanofluids. Energy Convers Manag 2011;52:789–793. [CrossRef]

[19] Datta A, Halder P. Thermal efficiency and hydraulic performance evaluation on Ag-Al2O3 and SiC-Al2O3 hybrid nanofluid for circular jet impingement. Arch Thermodyn 2021;42:163–182.

[20] Datta A, Halder P. Curved surface and thermal performance factor effect using SiC-Al2O3 hybrid nanofluid jet impingement. Interfacial Phenom Heat Transf 2020;8:321–336. [CrossRef]

[21] Sahoo RR, Sarkar J. Heat transfer performance characteristics of hybrid nanofluids as coolant in louvered fin automotive radiator. Heat Mass Transf 2017;53:1923–1931. [CrossRef]

[22] Guo ZY, Li DY, Wang BX. A novel concept for convective heat transfer enhancement. Int J Heat Mass Transf 1998;41:2221–2225. [CrossRef]

[23] Bergles AE. Recent developments in enhanced heat transfer. Heat Mass Transf 2011;47:1001–1008. [CrossRef]

[24] Guo ZY, Tao WQ, Shah RK. The field synergy (coordination) principle and its applications in enhancing single phase convective heat transfer. Int J Heat Mass Transf 2005;48:1797–1807. [CrossRef]

[25] Tao WQ, Guo ZY, Wang BX. Field synergy principle for enhancing convective heat transfer— its extension and numerical verifications. Int J Heat Mass Transf 2002;45:3849–3856. [CrossRef]

[26] Minea AA, Manca O. Field-synergy and figure-of-merit analysis of two oxide–water-based nanofluids' flow in heated tubes. 2017;38:909–918. [CrossRef]

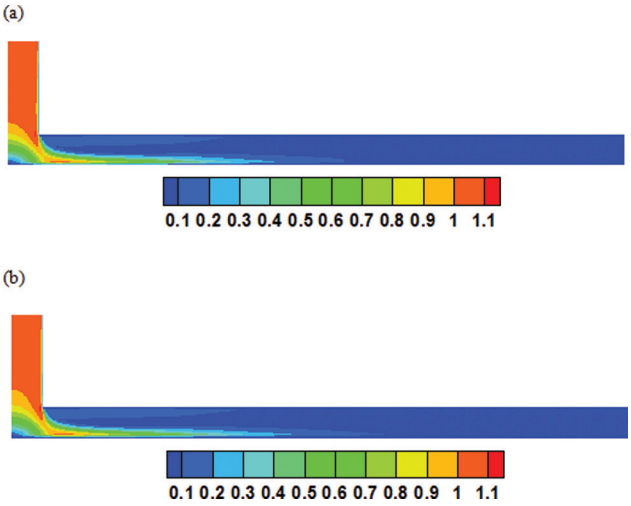

Figure A1. Temperature contour ((a) Re = 10000, f = 4%, H/D = 1, (b) Re = 40000, f = 4%, H/D = 1).

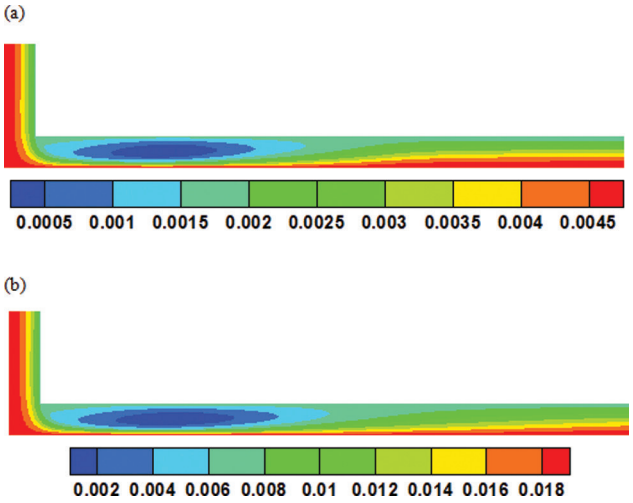

Figure A2. Streamline contour ((a) Re = 10000, f = 4%, H/D = 1, (b) Re = 40000, f = 4%, H/D = 1).

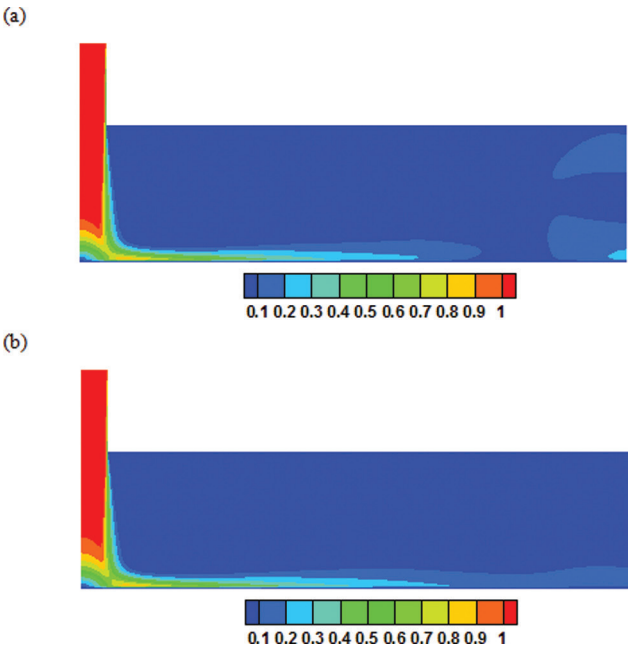

Figure A3. Temperature contour ((a) Re = 10000, f = 4%, H/D = 5, (b) Re = 40000, f = 4%, H/D = 5).

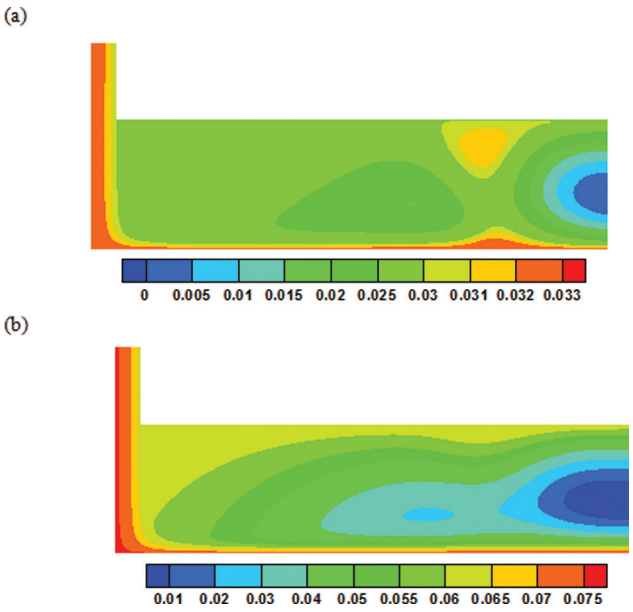

Figure A4. Streamline contour ((a)Re = 10000, f = 4%, H/D = 5, (b)Re = 40000, f = 4%, H/D = 5).